ICAS 2021 SHANG HAI
32nd Congress of the International Council of the Aeronautical Sciences
September 6-10, 2021 Pudong Shangri-La, Shanghai, China

ACTIVITY CHARACTERISTICS AND THE MECHANISM OF MESO-MICRO SCALE DISTURBANCES IN THE EAST ASIAN SUBTROPICAL UPPER-LEVEL JET STREAM

Chen Xian[1], Huang Jiangtao[1], Meng Meng[2], Chen Cheng[1] & Chen Qisheng[1]

[1]China Aerodynamics Research and Development Center, Mianyang, Sichuan, 621000
[2] Wenzhou Meteorological Burea, Wenzhou, Zhejiang, 325000

Abstract

The disturbance inside the East Asian subtropical upper-level jet stream is a kind of extremely dangerous weather phenomenon for aviation safety. However, activity characteristics and the mechanism of meso-micro scale disturbances are still unclear. In this paper, we use the high spatial-temporal resolution output and dynamic theories to study disturbances. The results indicate that the meso-micro scale disturbance activities may be predicted according to the characteristics of the inertial gravity wave.

Keywords: The East Asian Subtropical Upper-Level Jet Stream; Numerical Simulation; Disturbance; Inertial Gravity Wave; Atmospheric Stability

1. Introduction

The East Asian subtropical upper-level jet (EASJ) is a long and narrow airflow located in the upper troposphere and the lower stratosphere [1]. The EASJ is the most intense jet in the world. The wind speed around the EASJ axis can reach over 100 m/s. The EASJ is characterized by large wind shears both in horizontal and vertical directions due to its special spatial structure, leading to many meso-micro scale disturbances inside it [2-3]. Moreover, the altitude of EASJ axis is approximately equal to the cruise altitude of aviation aircrafts. As a result, the disturbances inside the EASJ are one of extremely dangerous weather for aviation safety [4]. However, disturbances often take place without visible weather phenomenon and cannot be detected by present airborne radar [5]. Consequently, it is difficult to predict the disturbance activities. Therefore, it is of great importance to clarify activity characteristics and the mechanism of meso-micro scale disturbances in the EASJ.

It is known to all that the theoretical analysis can only give qualitative criteria for the genesis and development of disturbances. The horizontal structure of disturbances cannot be acquired from sounding data. Moreover, the upper-level three-dimensional high spatial-temporal resolution sounding data is very difficult to obtain. Therefore, the high-resolution numerical model for atmospheric simulation has become a useful tool for studying meso-micro scale disturbances in the EASJ. In this paper, a case study is conducted to investigate the activity characteristics of the disturbances in the EASJ and the corresponding physical mechanism based on numerical experiments.

2. Experimental design and simulation verification

2.1 Experimental design

In this paper, the Weather Research and Forecasting (hereafter WRF) model (version 3.4.1) is used to simulate the East Asian regional circulation from July 1, 00:00 Universal Standard Time (hereafter UTC) to July 16, 00:00 UTC, 2003. The WRF is a kind of non-hydrostatic mesoscale numerical weather prediction system, which is designed for both atmospheric research and operational forecasting applications. The experiment two-domain one-way nested grids with the

respective horizontal resolutions of 30 km and 10 km, and covers squared domains of 3000×3000 km^2 and 1330×1330 km^2, respectively. The centers of two domains are both located at (130°E, 39°N). The model top is 50hPa with 51 vertical levels. The large-scale driven field of the WRF is extracted from the National Centers for Environmental Prediction (NCEP)/ the National Centers for Atmospheric Research (NCAR) reanalysis product on global 1°×1° grids (https://doi.org/10.5065/D6M043C6). The lateral boundary forcing is updated at 6-h intervals. The integration time step is 90 seconds and 30 seconds for coarse and fine domain, respectively. The time interval for the model output is 6 minutes. The important physical schemes include the WSM 5-class microphysics scheme and the Kain-Fritsch (New Eta) cumulus parameterization scheme in coarse domain, and the Thompson microphysics scheme and the Grell 3D ensemble cumulus parameterization scheme in fine domain. Other physical schemes, which are the same in coarse and fine domains, contain the RRTM long-wave radiation scheme, the Dudhia short-wave radiation scheme, the YSU planetary boundary scheme, the Unified Noah land surface scheme, and the Monin-Obukhov similarity theory for surface layer physics. Detailed description of the WRF dynamics and physical schemes can be found in Skamarock et al. [6].

2.2 Simulation verification

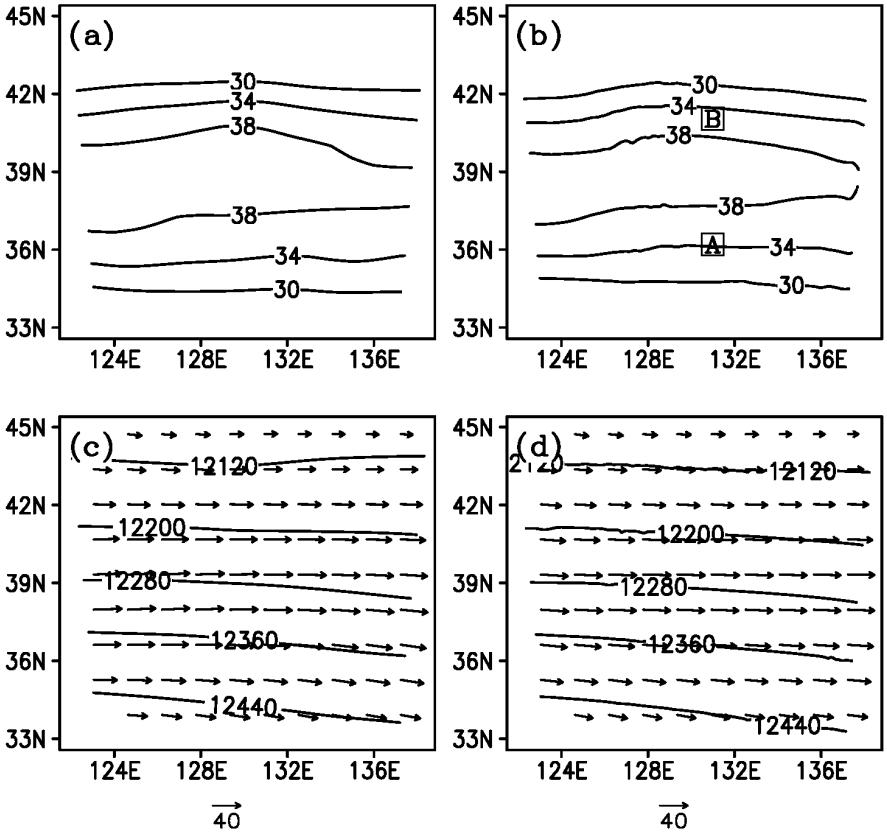

Figure 1 Observed (a, c) and simulated (b, d) regional circulations during the integration period: (a) and (b) Mean wind speed at 200 hPa (solid line, unit: m/s); (c) and (d) Mean geopotential height (solid line, unit: gpm) and wind field (vector, unit: m/s) at 200 hPa.

Figure 1 exhibits the observed and simulated regional circulations at 200hPa during the integration period. Comparing Figure 1a and 1b, it can be found that the WRF model can well simulate intensity and distribution of the EASJ. The largest wind speed of the EASJ in observation and simulation are both 39 m/s and located near the 39°N. The simulated geopotential height and wind vectors are almost identical to those of observed (Figure 1c and 1d). Moreover, the spatial

correlation coefficients between observed and simulated regional circulations during the integration period are above 0.90. Consequently, the simulation can well represent variance characteristics of the EASJ. Next, the simulations are used to analyze activity characteristics of meso-micro scale disturbances and the corresponding mechanism.

3. Results

As is shown in Figure 1c, the EASJ case we studied is the latitudinal distribution type. The zonal wind speed of the EASJ case is far greater than the meridional wind speed. Thus, the following studies on the evolution of the EASJ are mainly based on the zonal wind component.

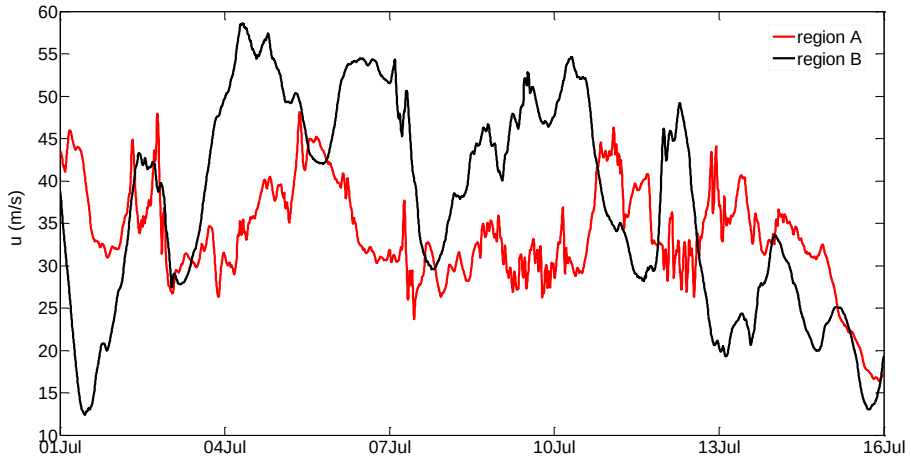

Figure 2 Time series of averaged zonal wind in region A and B during the integration period.

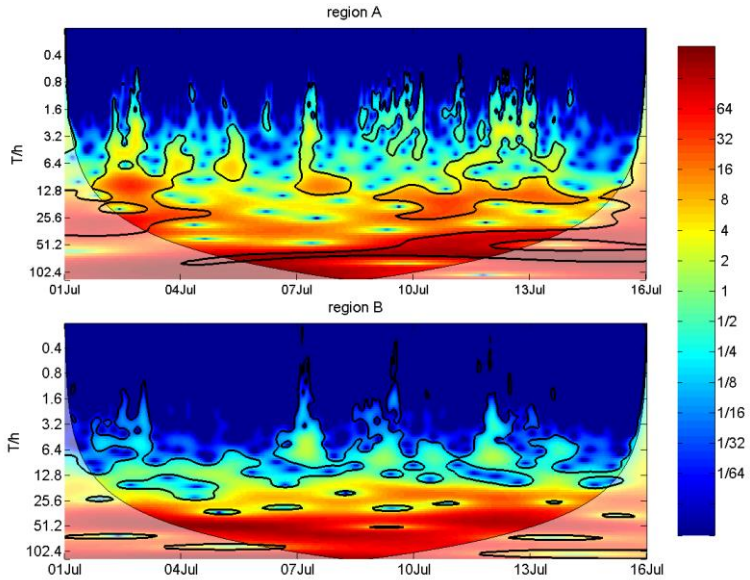

Figure 3 Wavelet power spectrum of averaged zonal wind time series in region A and B, where the thick black contours represent the 95% confidence level.

Region A and B shown in Figure 1b, with an area of 0.5°×0.5°, are centered on the South (131°E, 36°N) and North (131°E ,41°N) sides of the EASJ, respectively. Time series of averaged zonal wind in region A and B during the integration period are represented in Figure 2. As is shown in the Figure, the wind speed is oscillating both in area A and B. However, the wind speed in area A seems more variable than that in area B. For example, from July 7 to 13 the frequency of wind speed variation is far higher in region A than that in region B. To further study the evolution characteristics of the EASJ, a Morlet wavelets program supplied by Torrance and Compo [7] is

used to do time-frequency decomposition for the variability of zonal wind in region A and B. The wavelet power spectrum of averaged zonal wind time series in region A and B is exhibited in Figure 3.

It is found that, the zonal wind in region A, with its dominant period shorter than 12 hours, shows significant high-frequency variations with periods less than 1 hour in almost every day. However, there are only three high-frequency variations occur in region B. Furthermore, the dominant period of the zonal wind in region B is longer than 12 hours. Consequently, the high-frequency disturbances are more likely to occur in the south of the EASJ.

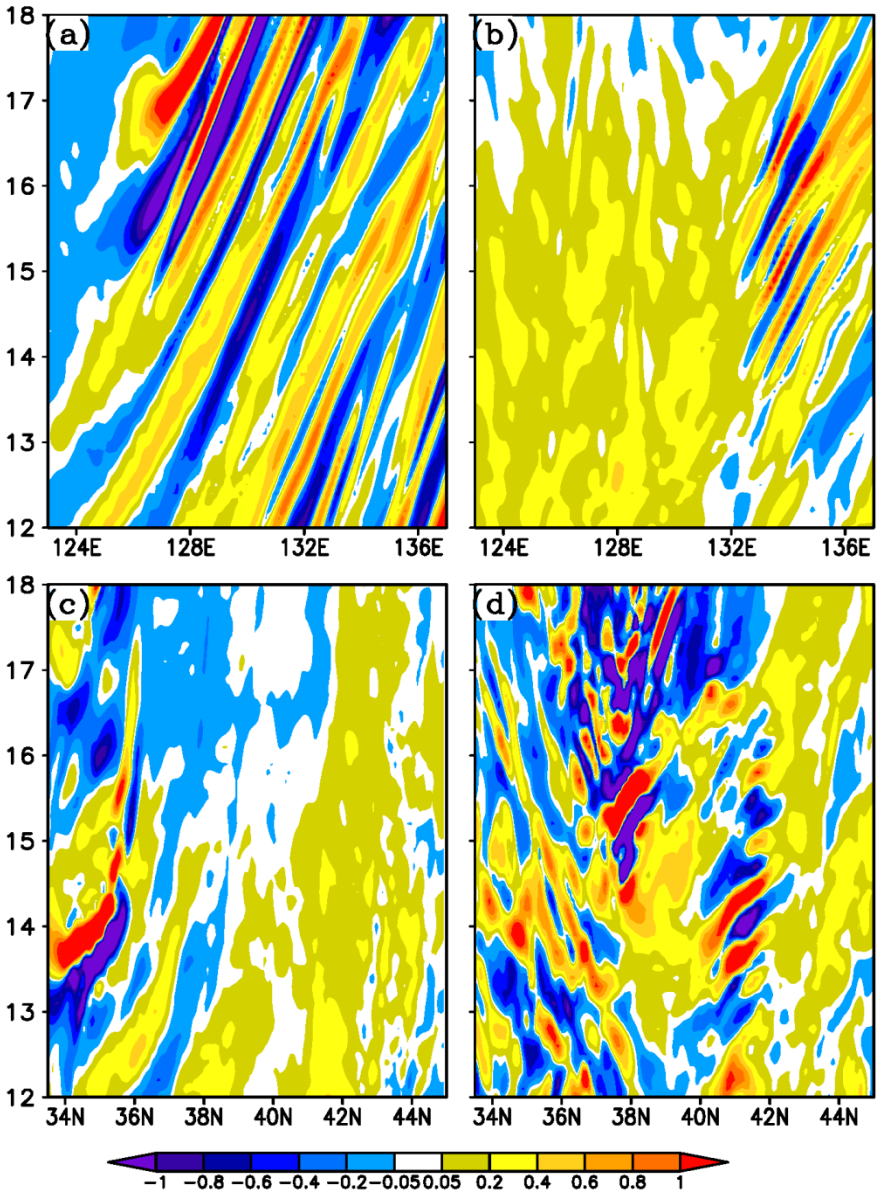

Figure 4 The time-longitude sections along (a) 36°N, (b) 42°N and the time-latitude sections along (c) 126°E, (d) 133°E of zonal wind increment (shaded, unit: m/s) at 6 minutes interval at 200hPa during 12:00 UTC to18:00 UTC July 9, 2003.

Previous studies show that the characteristics of transient disturbance in the EASJ can be characterized by the wind speed increment of two sequential times [8-9]. Therefore, we use the increment of zonal wind to reveal the characteristics of short time scale disturbance. The distribution of increment can represent the horizontal scale of disturbance, and the time interval of positive and

negative wind direction variations can represent the period of disturbance evolution.
The increment of zonal wind is defined as follow:

$$\delta u(x,y,z,t) = u(x,y,z,t+\delta t) - u(x,y,z,t) \quad (1)$$

Where u is the zonal wind component, and δt =6 minutes is the time interval for the model output.
Figure 4 shows the time-longitude sections along 36°N, 42°N and the time-latitude sections along 126°E, 133°E of zonal wind increment at 6 minutes interval at 200hPa during 12:00 UTC to 18:00 UTC July 9, 2003. It is shown that the zonal wind increment on the south side of the jet axis presents an obvious fluctuation characteristic with time (Figure 4a). There are about 6 times of fluctuation shifts in the EASJ within 6 hours, indicating that the period of atmospheric wave is about 1 hour in the south side of the EASJ. Moreover, it can be estimated that the wave propagates eastward at a speed of about 20-40 m/s. In the north side of the jet axis, there are similar high-frequency disturbances in the zonal wind increment, but the high-frequency disturbances are less than those in the south side, with a period of about 2-6 hours, and have the characteristics of eastward propagation (Figure 4b). Compared with Figure 4c and Figure 4d, it can be seen that in the west section of the jet stream, the high-frequency disturbance is mainly located in the south side of the jet stream axis, while in the east section, there are high-frequency disturbances on both north and south sides of the jet stream axis, but the high-frequency disturbances in the south side of the jet stream axis is more obvious. The above results show that the south side of the jet axis is more favorable for high-frequency disturbances generation than the north side. The period of change and propagation velocity of these high-frequency disturbances are close to the period and phase velocity of the inertial gravity wave respectively [9-10], indicating that these high-frequency disturbances may be related to the inertial gravity wave.

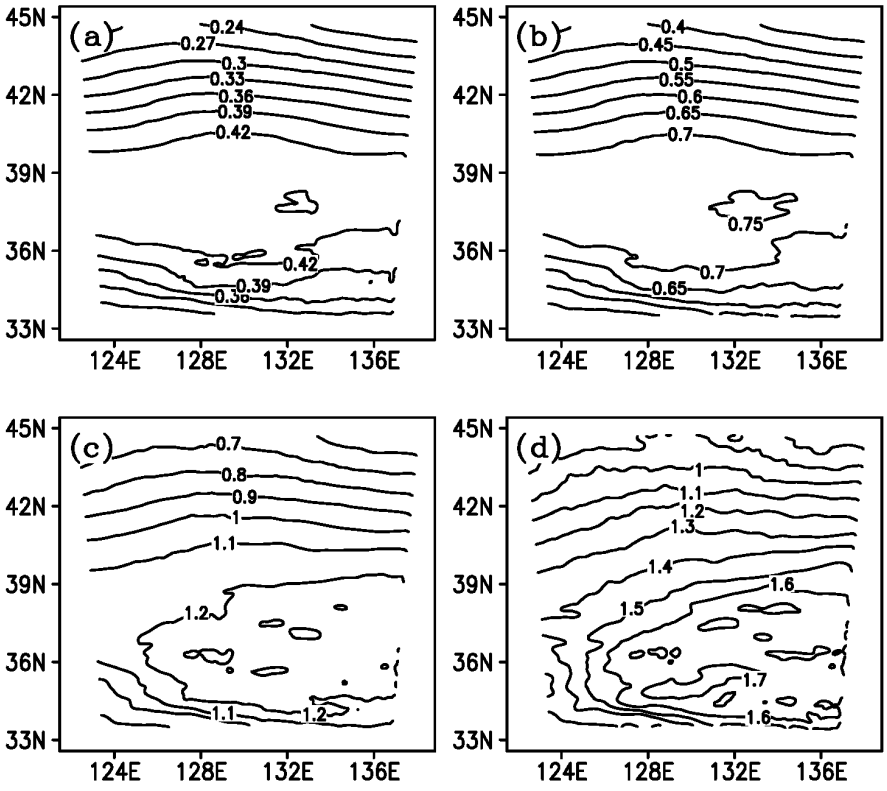

Figure 5 The root-mean-square of the velocity fluctuation during the integration period, where the period of the velocity fluctuation is shorter than (a) 30 minutes, (b) 1 hour, (c) 3 hours, and (d) 6 hours, respectively.

The root-mean-square of the velocity fluctuation is often used to indicate the intensity of turbulence:

$$V'(x,y,z)=\frac{1}{n}\sum_{t=1}^{n}\sqrt{u'^2(x,y,z,t)+v'^2(x,y,z,t)} \tag{2}$$

Where V' is the root-mean-square of the velocity fluctuation, u' and v' are meridional and zonal velocity fluctuation, respectively, and n is the number of the model outputs during the integration period. The root-mean-square of the velocity fluctuation during the integration period is shown in Figure 5.

As is shown in Figure 5a, the maximum of velocity fluctuation root-mean-square is located around 38°N. The magnitude of velocity fluctuation root-mean-square in the south of the EASJ is larger than that in the north. Moreover, distributions of root-mean-squares of the velocity fluctuation with period shorter than 1 hour, 3hours and 6 hours are similar to that shown in Figure 5a (Figure 5b, 5c and 5d). The magnitude of maximum velocity fluctuation root-mean-square is about 2 times as much as that in the north of the EASJ. The above results show that the intensity of atmospheric turbulence in the south side of the EASJ is much greater than that in the north side of the EASJ.

4. Mechanism

According to the theory of geostrophic adaptation, the ageostrophic flow can excite the inertial gravity wave [11-12]. Furthermore, Zhang et al. [13] pointed out that the Lagrange Rossby number is a main index to diagnose the ageostrophic characteristics of atmospheric circulation.

At 200hPa, the friction is negligible. As a result, the atmospheric motion equation can be simplified as follows:

$$\frac{d\vec{V}}{dt}=f\vec{V}_{ag}\times\vec{k} \tag{3}$$

Where $\vec{V}$ is the wind vector, $\vec{V}_{ag}$ is the geostrophic deviation, and f is the Coriolis force. The Lagrange Rossby number is defined as follows:

$$R_0=\frac{|d\vec{V}/dt|}{f|\vec{V}|} \tag{4}$$

As is shown in eq (3), R_0 indicates the proportion of the geostrophic deviation in the wind speed. According to Koch et al. [14], the wind flow is ageostrophic when R_0 is larger than 0.5.

The Richardson number is often used as a criterion to judge whether convection or turbulence can develop or not [14-15]:

$$Ri=\frac{N^2}{\left(\frac{pg}{RT}\right)^2\left[\left(\frac{\partial u}{\partial p}\right)^2+\left(\frac{\partial v}{\partial p}\right)^2\right]} \tag{5}$$

$$N^2=-\frac{pg^2}{RT}\frac{\partial\ln\theta_0}{\partial p} \tag{6}$$

The smaller the Ri is, the easier turbulence is to develop.

The time-latitude sections along 133°E of Lagrange Rossby number and Richardson number at 200hPa are shown in Figure 6.

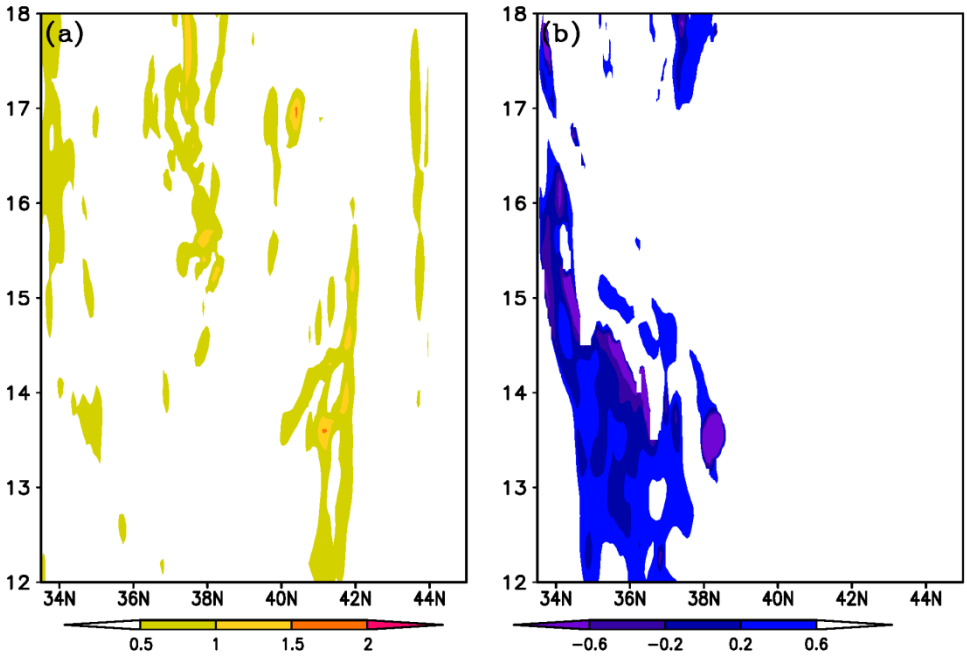

Figure 6 The time-latitude sections along 133°E of (a) Lagrange Rossby number and (b) Richardson number at 200hPa during 12:00 UTC to18:00 UTC July 9, 2003.

It is found that the Lagrange Rossby number is larger than 0.5 in both side of EASJ axis when disturbances occur in the EASJ region, indicating that disturbances and the ageostrophic flow are closely related (Figure 6a). As is known to all, the ageostrophic state is an advantage for the foundation and development of inertial gravity wave. Consequently, the inertial gravity wave may be a main source of the disturbances in the EASJ. Moreover, it is shown in Figure 6b that the Richardson number is smaller in the south of the EASJ when the disturbances occur, so the shearing instability is more likely to occur there. The instability may lead the gravity waves in the south of the EASJ axis to break up and develop into smaller disturbances.

5. Conclusion and discussion

The above results show that the disturbances in the EASJ are closely related to the inertial gravity wave. Due to the low atmospheric stability in the south of the EASJ, the inertial gravity waves in that region are more likely to break up and develop into smaller disturbances. Therefore, the period of the circulation variation is much shorter in the south of the EASJ. These high-frequency disturbances seem to be more dangerous as the intensity is stronger. As a result, the Lagrange Rossby number and the Richardson number can be used as indices to predicted the meso-micro scale disturbance activity in the EASJ.

6. Contact Author Email Address

Corresponding author: Huang Jiangtao; E-mail: hjtcyf@163.com

7. Copyright Statement

References

[1] Zhang Y, Kuang X, Guo W and Zhou T. Seasonal evolution of the upper-tropospheric westerly jet core over East Asia. *Geophysical Research Letters*, Vol. 33, pp L11708, 2006.

[2] Kim J H and Chun H Y. A numerical study of Clear Air Turbulence (CAT) encounters over South Korea on 2 April 2007. *Journal of Applied Meteorology and Climatology*, Vol. 49, No.12, pp 2381-2403, 2010.

[3] Deng S G, Zhong Z, and Cheng H H. Evolution characteristics of gravity-wave parameters in a simulated rainstorm process. *Chinese Journal of Geophysics* (in Chinese), Vol. 55, No.6, pp 1831-1843, 2012.

[4] Williams P D. Increased light, moderate, and severe clear-air turbulence in response to climate change. *Advances in Atmospheric Sciences*, Vol. 34, No.005, pp 576-586, 2017.

[5] Storer L N, Williams P D, and Joshi M M. Global response of clear-air turbulence to climate change. *Geophysical Research Letters*, Vol.44, No.19, pp 9976-9984, 2017.

[6] Skamarock W C, and Coauthors. A Description of the Advanced Research WRF Version 3. *NCAR Technical Note NCAR/TN-475+STR*, 2008.

[7] Torrence C, and Compo G P. A Practical Guide to Wavelet Analysis. *Bulletin of the American Meteorological Society*, Vol.79, No.1, pp 61-78, 1998.

[8] Chang E K M, and Fu Y. Interdecadal variations in Northern hemisphere winter storm track intensity. *Journal of Climate*, Vol.15, No.6, pp 642-658, 2002.

[9] Zhong Z, Yuan H H, Li J, and Fan H Y. Characteristics of the meso-scale perturbations and momentum transportation associated with an intensification process of upper-level jet. *Journal of the Meteorological Sciences* (in Chinese), Vol.30, No.5, pp 639-645, 2010.

[10]Deng S G, Zhong Z, and Cheng H H. Evolution characteristics of gravity-wave parameters in a simulated rainstorm process. *Chinese Journal of Geophysics* (in Chinese), Vol.55, No.6, pp 1831-1843, 2012.

[11] Rossby C G. On the mutual adjustment of pressure and velocity distributions in certain simple current systems I. *Journal of Marine Research*, Vol.1, pp 15-28, 1937.

[12] Rossby C G. On the mutual adjustment of pressure and velocity distributions in certain simple current systems II. *Journal of Marine Research*, Vol. 2, pp 239-263, 1938.

[13] Zhang F Q, Koch S E, Davis C A, and Kaplan M L. A survey of unbalanced flow diagnostics and their application. *Advances in Atmospheric Sciences*, Vol.17, No.2, pp 165-183, 2000.

[14] Koch S E, and Dorian P B. A mesoscale gravity wave event observed during CCOPE. Part III: wave environment and probable source mechanisms. *Monthly Weather Review*, Vol.116, No.12, pp 2570-2592, 1988.

[15] Koch S E, and Coauthors. Turbulence and gravity waves within an upper-level front. *Journal of the Atmospheric Sciences*, Vol.62, No.11, pp 3885-3908, 2005.